HHS Public Access

Author manuscript

Expert Rev Ophthalmol. Author manuscript; available in PMC 2016 April 13.

Published in final edited form as:

Expert Rev Ophthalmol. 2015 ; 10(2): 183–195. doi:10.1586/17469899.2015.1012500.

Evaluating glaucoma damage: emerging imaging technologies

Tigran Kostanyan[1], **Gadi Wollstein**[*,1], and **Joel S Schuman**[1,2]

[1]Department of Ophthalmology, UPMC Eye Center, Eye and Ear Institute, Ophthalmology and Visual Science Research Center, University of Pittsburgh School of Medicine, Pittsburgh, PA, USA

[2]Department of Bioengineering, Swanson School of Engineering, University of Pittsburgh, Pittsburgh, Pennsylvania, PA, USA

Abstract

The use of ocular imaging tools to estimate structural and functional damage in glaucoma has become a common clinical practice and a substantial focus of vision research. The evolution of the imaging technologies through increased scanning speed, penetration depth, image registration and development of multimodal devices has the potential to detect the pathology more reliably and in earlier stages. This review is focused on new ocular imaging modalities used for glaucoma diagnosis.

Keywords

Glaucoma; Spectral Domain OCT; Swept Source OCT; Adaptive Optics; Polarization Sensitive OCT; OCT Blood Flow; OCT Aqueous Humor Outflow; Phase Sensitive OCT

Introduction

Glaucoma is a multi-factorial neurodegenerative disease characterized by loss of retinal ganglion cells (RGC) and their axons, resulting in noticeable changes in the optic nerve head (ONH) and retinal layers, and accompanied by visual function deterioration. Glaucoma is the second leading cause of blindness worldwide, and by 2020 there will be 3.36 million individuals affected by open angle glaucoma in the United States.[1] The early detection of this slowly progressive pathology is crucial because glaucomatous vision loss is irreversible and an appropriate treatment can potentially slow disease progression and preserve vision.

Glaucoma is diagnosed by the detection of characteristic functional and structural changes. The subjective nature of glaucoma detection with legacy methods such as automated perimetry and stereoscopic disc photography led clinicians, researchers, and engineers to develop and study technologies that could provide objective and reliable estimation of

[*]Author for correspondence: wollsteing@upmc.edu.

Financial & competing interests disclosure

JS Schuman receives royalties for intellectual property licensed by Massachusetts Institute of Technology to Zeiss. The authors have no other relevant affiliations or financial involvement with any organization or entity with a financial interest in or financial conflict with the subject matter or materials discussed in the manuscript apart from those disclosed.

glaucomatous structural damage. The evolution of ophthalmic imaging tools during the past two decades has enabled the acquisition of in-vivo and real time objective, accurate, quantitative, and precise measurements of the ONH, the retinal nerve fiber layer (RNFL), and macular substructures.

Currently, glaucoma imaging research and development is mostly focused on imaging tools with higher scanning speeds, higher axial and transverse resolution, the ability to simultaneously estimate both structural and functional characteristics of scanned tissue, new automated algorithms for image registration, segmentation, and analysis, and tools that allow sensitive detection of glaucoma progression.

The purpose of this manuscript is to review the progress in ocular imaging development within the past five years and to discuss promising future trends.

Optical Coherence Tomography

Optical Coherence Tomography (OCT) uses the principle of low-coherence interferometry and is able to obtain in-vivo structural information from scanned tissue on a micrometer level. The technology was first described in 1991[2] and has since evolved significantly and gained leading positions in ocular imaging.

The first generation of OCT, known as time-domain OCT (TD-OCT), analyzes information from the echo-time delay of back reflected near-infrared light.[3] The structural measurements of the scanned tissue are generated by comparing the location of each reflection to the position of a moving reference mirror. The scanning speed of this technology is limited to 400 axial scan/sec, due to the maximal oscillating speed of the reference mirror.[4]

The next generation of OCT, the Fourier domain or spectral-domain (SD-) OCT, was introduced in 2001.[5] The fundamental difference of this method is the use of light frequency information instead of time delay data to determine the spatial location of reflected light. This technology is capable of simultaneously acquiring all of the information in a single axial scan through an area of interest by analyzing the frequency information of the interference between the reflected light and a stationary reference mirror. This improvement results in a substantial increase in scanning speed, up to 75,000 axial scans/sec in commercially available devices and up to 20,8 million scans/sec in research devices.[6]

The widespread use of OCT in glaucoma detection and monitoring is due to the high reproducibility of the automated measurements of the retinal layers and ONH as demonstrated in many studies[7],[8],[9],[10],[11], and because it has a high ability to discriminate between healthy and glaucomatous eyes.[12],[13],[14],[15],[16],[17],[18],[19]

Several studies demonstrated that there is no significant difference in glaucoma diagnostic capabilities between TD-OCT and SD-OCT[20],[21],[*22], although the ongoing improvements in SD-OCT technology are likely to shift that balance. The main parameters that OCT machines use to discriminate glaucomatous structural damage are peripapillar RNFL thickness, ONH parameters, and macular measurements.[7],[23]

Despite using the same basic principles of SD-OCT technology, the built-in automatic glaucoma protocols of different commercially available devices use different algorithms to acquire and analyze structural scans. This makes the comparison of scans and measurements acquired with different devices a challenging task.

Retinal Nerve Fiber Layer

RNFL thickness was the first parameter used for the estimation of glaucomatous structural damage in OCT technology.[24] The advantage of this parameter is the ability to sample axons from the entire retina on their approach to the ONH. RNFL thickness is primarily measured from a peripapillary circle centered on the optic disc head. The default setting of this circle, a 3.4 mm fixed diameter, is placed at a location with a relatively stable RNFL thickness, allowing for *small* variations in the exact circle placement without causing a substantial difference in the overall thickness.[25]

Fast scanning speed devices, such as SD-OCT and more recent OCT technologies, enable the use of dense scanning patterns such as the raster scan, allowing the construction of a 3-dimensional (3D) cube using all of the measurements from the entire scanning region. This allows the provision of the RNFL thickness information in two ways: through circumpapillary RNFL mapping similar to the method described above, that can be generated from the 3D cube of data, or a RNFL thickness map of the entire peripapillary region. Acquiring 3D data have another advantage as it allows precise registration of scans acquired over time, reducing the variability caused by slight differences in the tissue sampling location.[26]

The circumpapillary RNFL thicknesses provided by the SD-OCT devices are average RNFL thickness, thickness in four quadrants (temporal, superior, nasal, and inferior), and sectoral thickness at each of 12 to 16 equal size sectors. The RNFL thickness profile mostly follows the ISNT rule, with thickest RNFL in the inferior quadrant followed by the superior, nasal and temporal quadrants.[27]

The SD-OCT technology demonstrates excellent intravisit and intervisit RNFL measurement reproducibility; with the average RNFL thickness being the best parameter with a test-retest variability of 4.5μm to 6.05μm in different studies. [10],[26],[28],[29],[30]

Several studies demonstrated RNFL thickness variability with age, race, ethnicity, optic disc size, and axial length of the eye.[27],[31], [32] This should be taken in consideration when defining RNFL thickness pathologic changes.

The Cirrus HD-OCT (Zeiss, Dublin, CA) ONH and RNFL protocols collect the information from a 200 (height) ×200 (width) ×1024 (depth) point parallelepiped that is obtained within a 6×6×2mm cube centered on the ONH. RNFL measurements are compared with an age-matched normative database, and the areas below the lower 95% normal distribution range in each location are highlighted [Figure 1]. RNFL parameters are presented as a color-coded map with green, yellow, or red representing locations with RNFL thickness within normal range, < 5% and < 1%, respectively, in comparison with the normative database.

The Spectralis OCT (Heidelberg Engineering, Heidelberg, Germany) protocol generates a circumpapillary RNFL thickness map from a circle centered on the ONH. The actual thickness values and color-coded comparison results are presented as global average thickness, thickness in four quadrants, and thickness in six sectors [Figure 2].

RTVue Premier (Optovue, Fremont, CA) obtains 13 concentric circumpapillary scans with diameters of 1.3 – 4.9 mm and 12 radial linear scans 3.7 mm in length centered on the ONH to create a peripapillary map. The comparison with the normative database is conducted in 16 sectors and as a deviation map.

The different scanning protocols of the variety of commercially available OCT devices lead to variability in RNFL thickness measurements. A study that included glaucoma, glaucoma suspect, and healthy eyes examined the agreement of RNFL thickness measurements obtained with three commercially available SD-OCT devices (Cirrus HD-OCT, Spectralis OCT, and RTVue OCT).[33] The results showed significant RNFL thickness measurement difference between the devices. The RNFL measurements acquired with RTVue were thicker than Cirrus HD-OCT and Spectralis OCT. Significant differences in RNFL thickness measurements between Cirrus HD-OCT and Spectralis OCT were reported, with Spectralis values being higher in all quadrants except nasal.[34]

The best RNFL parameters to distinguishes between glaucomatous and healthy eyes are the RNFL thickness at the inferior temporal clock-hour 7, superior-temporal region, inferior quadrant, and average RNFL thickness.[13],[35] Glaucoma diagnostic capability of RNFL clock hour and quadrant thickness maps, and the deviation map was assessed in eyes with localized RNFL defect.[36] The results demonstrated that the RNFL deviation map is more sensitive in detecting RNFL defects than the clock hours and quadrant maps obtained by TD-OCT and Cirrus HD-OCTs. This result emphasizes the importance of assessing the deviation map for the most sensitive detection of glaucomatous damage.

Novel algorithms to improve the alignment of subsequent scans and to minimize the movement artifacts were recently incorporated into commercial OCT system. This method connects two fixed landmarks (the center of the fovea and the center of the Bruch’s membrane opening (BMO)) to ensure consistent alignment of the optic nerve region, reducing measurements variability due to torsional movement.[37]

Optic Nerve Head

OCT technology can provide quantitative ONH assessments with parameters such as disc area, rim area, rim volume, vertical cup-to-disc ratio, horizontal cup-to-disc ratio, cup area, cup volume, and others. The acquisition of 3D images of the ONH region with SD-OCT results in accurate and reproducible measurements.[38],[39] Similar to RNFL thickness, the scanning protocols for the ONH also differ between the commercially available SD-OCT devices. The ONH parameters provided by Cirrus HD-OCT are generated from the 3D ONH scan described in the RNFL section above. Spectralis OCT provides ONH parameters by performing radial scans centered on the optic disc. The ONH protocol of RTVue Premier consists of a combination of radial and concentric circular scans as described above. Gaps

between the scans are interpolated. The ONH parameters are compared with normative data in several of the commercially available devices.

TD-OCT's ONH parameters has been shown to vary with disc area, age, intraocular pressure, axial length, lens nuclear color, and signal strength when measured in healthy eyes.[40] Similarly, SD-OCT measurements of ONH, RNFL, and macula in healthy eyes were shown to vary with age and ethnicity.[41]

The glaucoma diagnostic capabilities of ONH parameters acquired with early generation, TD-OCT and RTVue OCT were compared. The results demonstrated excellent agreement between both OCT devices with stereophotography with intraclass correlation coefficient (ICC) of 0.80 to 0.86, and excellent agreement of all ONH parameters between the two OCT devices. The ONH parameters obtained with both OCTs performed similarly in distinguishing glaucomatous damage.[42]

The ONH parameters that best discriminate between healthy and glaucomatous eyes are rim area, vertical rim thickness, vertical cup-to-disc ratio, and cup-to-disc area ratio.[13],[43] No statistically significant difference was noted between AUCs for the best ONH parameters and RNFL thickness measurements. Comparing the ability to discriminate between healthy and perimetric glaucomatous eyes with RNFL thickness measurement and ONH parameters showed superior performance of RNFL.[44] However, RNFL thickness and rim area showed similar diagnostic capability in advanced glaucoma.[13],[44]

Glaucoma diagnostic ability of new structural markers has been recently studied and incorporated in commercial OCT systems. Neuroretinal rim measurements using Bruch's membrane opening (BMO) base minimum rim width has the potential to improve glaucoma discrimination abilities of OCT systems.[45] This method measures the shortest distance between the BMO and the surface instead of the method that connects the optic nerve head boundary with the surface vertically anterior to it.

Macula

Taking into consideration that more than half of all RGCs are located in the macula and arranged in 7 to 8 cell layers,[46] this area is a valuable location for assessing glaucomatous damage.[47],[48],[49],[50] SD-OCT allows the acquisition of high quality images of this region, enabling advanced automated segmentation of retinal layers that has demonstrated high reproducibility.[50],[51] The layers of particular interest for glaucoma damage detection are macular RNFL (mRNFL), the ganglion cell layer with inner plexiform layer (GCIPL), and the ganglion cell complex (GCC = mRNFL + GCIPL), as these are the layers that are directly prone to glaucomatous damage.[52]

The Cirrus HD-OCT quantifies the GCIPL thickness by automatically segmenting these layers in an ellipse (vertical radius of 2 mm, horizontal radius of 2.4 mm) centered on the fovea, and displays the values on a color-coded thickness map [Figure 3]. Other specific parameters, such as average and minimum GCIPL thicknesses, sectoral maps, and deviation maps are compared with a normative age-matched database and presented as numerical and color-coded data.

The Spectralis OCT system provides values of total macular thickness within a 30° × 25° scan area centered on the fovea. The results are displayed using a color-coded gray scale. The current algorithm does not provide a comparison of macular thickness measurements to an age-matched normative database.

The macula protocol of RTVue Premier analyses the GCC that unlike other devices, includes the mRNFL thickness in addition to the GC-IPL thickness. The data is captured from a 7 mm^2 area centered 1 mm temporal to the fovea. The macular values are displayed on a color-coded thickness map and the algorithm provides RNFL deviation and significance maps for better visualization of glaucomatous damage [Figure 4]. The specific pattern of GCC loss is used to calculate the global and focal volume loss parameters.

A study that used Cirrus HD-OCT examined 138 healthy, ocular hypertensive, or glaucomatous eyes and reported highly reproducible GCIPL thickness measurements.[53]

Recent studies demonstrated that the glaucoma diagnostic capabilities of GCIPL were comparable with RNFL and ONH parameters.[18],[54],[55] Moreover, of the several examined GCIPL parameters (average, minimum, sectoral) the highest sensitivity was observed with the minimal GCIPL thickness.[51],[55] A study with Cirrus HD-OCT reported a similar AUC for GCA protocol, RNFL, and ONH analyses.[54] Similar performance was reported with Spectralis SD-OCT macular analysis and RNFL parameters to estimate glaucomatous damage.[56]

The visualization of posterior segment deeper structures such as choroid [59] and lamina cribrosa [60],[61] with commercial SD-OCT devices were reported using the enhanced depth imaging (EDI) scanning approach. However, the penetration depth of the technology is limited by the wavelength of the light source used with this technology.

Swept source OCT

Swept source OCT (SS-OCT) is a recent development in OCT technology where frequency information is acquired by sweeping a narrow bandwidth source through a broad range of frequencies.[57],[58] Most SS-OCT devices have a longer center wavelength of ~1310nm, compared with a wavelength of ~840nm in SD-OCT. This slightly reduces the image resolution but improves the tissue penetration, allowing better visualization of structures such as the choroid, sclera, lamina cribrosa, and the anterior chamber angle.[62],[63],[*64], [**65],[66],[67] The SS technology is able to acquire up to 400,000 axial scans/sec, and avoids the signal drop-off with scanning depth observed with earlier generation OCTs.[7] This allows acquisition of good quality images spanning over a wider depth such as an image that contains the inner retina and the full choroid thickness in the same image [Figure 5].

Using a prototype SS-OCT device with an acquisition rate of 100,000 axial scans/sec and a central wavelength of 1030nm, good retinal and choroidal measurement repeatability was reported with high ICCs.[68]

The involvement of the lamina cribrosa in the glaucomatous process has been previously documented with histology. The improved specifications of SS-OCT enable in-vivo acquisition of high quality images of this structure. In a cross-sectional study of 182 glaucoma eyes the authors reported focal and full-thickness lamina cribrosa defects that corresponded with RNFL and neuroretinal rim thinning and visual field defects.[*64] Further investigating the lamina cribrosa involvement in glaucoma, an in-vivo SS-OCT study evaluated the *microarchitectural* differences between healthy and glaucomatous eyes using automated segmentation of the lamina cribrosa.[69],[**65] The authors documented lamina cribrosa changes that reflect beam remodeling with reduction in pore size and increased pore size variability. Using SS-OCT to assess ONH changes that appeared after glaucoma surgery, it has been reported that the percent change in the maximal LC depth is correlated with the percent change in IOP, baseline LC depth, and visual field mean deviation.[70]

The deep penetration of SS-OCT devices with a long wavelength has also been shown to be advantageous for the clinical assessment of the anterior segment of the eye. SS-OCT can accurately detect and quantify peripheral anterior synechia[71],[72], the width of the trabecular meshwork[73], and automatically quantifies the circumferential extent of the angle-closure-iris-trabecular contact index.[74],[72] This parameter had an AUC = 0.83 for differentiating between healthy and angle closure eyes as defined by gonioscopy.[75] Another method to identify angle closure used a machine learning technique with various descriptive anterior segment parameters generated from SS-OCT scans.[76] A study of 148 subjects identified fractal dimension (a complex shape descriptor quantifying irido-corneal angle characteristic) and a biometric parameter as the best combination to identify closed angle eyes with an accuracy rate of 99.1% and an AUC = 0.98.

Software enhancements in SS-OCT technology enable the performance of non-invasive angiography without the need of a contrast agent. SS-OCT with a split-spectrum amplitude-decorrelation angiography algorithm was used to estimate ONH perfusion in-vivo.[**77] A set cut-off of the optic disc flow index achieved a full separation between healthy and glaucomatous eyes (including a wide range of disease severity) with 100% sensitivity and specificity. Using multivariant analysis, the authors reported high correlation ($R^2 = 0.75$) between this parameter and visual field pattern standard deviation, which might open a new venue for disease detection and monitoring.

Adaptive optics

Adaptive optics (AO) is a well-established method to reduce the effect of wavefront distortions and is used to improve the performance of optical systems. The technique is based on the correction of the deformations of an incoming wavefront using a deformable mirror for compensation of the distortions. This method originates from astronomy imaging protocols used to correct for atmospheric and other optical aberrations and to enhance and resolve faint features. AO was successfully implemented into ocular imaging, boosting resolution and improving image quality.

A fundus camera coupled with AO are capable of obtaining in-vivo retinal images at the cellular level,[78] and are mostly used for retinal disease. A few studies have demonstrated the utility of the AO technique when coupled with scanning laser ophthalmoscopy (SLO) and OCT allowing to resolve in-vivo structures such as the retinal microvasculature, photoreceptors, ganglion cell, and the lamina cribrosa [Figure 6]. [79],[80]

Using AO coupled with a fundus camera and with SD-OCT, researchers examined cone photoreceptor density and the length of inner and outer segments of cone photoreceptors in subjects with glaucomatous and non-glaucomatous optic neuropathies.[81] They observed significant correlation between visual field sensitivity and the integrity of outer retinal layers, as well as the density of cone photoreceptors at corresponding locations. The photoreceptor outer segments were shorter, and exhibited greater variability in retinal areas associated with visual field losses compared with normal or less affected areas of the same patient's visual field. The results of another study supported the findings of outer retinal layer involvement in glaucomatous eyes.[*22] These studies were first to report the involvement of the outer retina in glaucoma.

AO-OCT technology was used to obtain cross-sectional images of individual nerve fiber bundles in four healthy eyes and one eye with a known arcuate RNFL defect.[*82] The study evaluated the reproducibility of acquired measurements, and compared the performance of the AO-OCT device with a commercially available SD-OCT device (Spectralis SD-OCT). The results showed the technology's ability to acquire reproducible measurements and the ability to provide superior microscopic retina visibility compared to the Spectralis SD-OCT. Moderate correlation ($r = 0.374$) between nerve fiber bundle width and RNFL thickness was observed in healthy and glaucomatous eyes.[80] The authors also reported that areas of the retina with a significantly lower nerve fiber bandwidth had corresponding defects in visual field even though RNFL thickness was preserved. These findings might suggest that evaluation of retinal structural damage on the microscopic level might be superior to retinal thickness in terms of glaucoma detection.

AO-OCT system was used to scan the lamina cribrosa in healthy, glaucoma suspect, and glaucomatous eyes. An automated segmentation analysis was used to quantify 3D lamina cribrosa microarchitecture that showed good measurement reproducibility.[83] This method creates the possibility of automated and comprehensive assessment of the lamina cribrosa that can be an important tool in understanding the glaucomatous process.

Polarization sensitive OCT

Polarization sensitive OCT (PS-OCT) technology generates images based on the polarization state altering properties of the examined structures. This technology provides both intensity information and the polarization sensitivity of the tissue. PS-OCT is capable of distinguishing individual retinal layers by their polarization properties, such as the birefringent of the RNFL and the depolarization of the RPE. This method has been recently incorporated into SD-OCT[84], SS-OCT[85], and AO-OCT[86].

A PS-OCT device that operates at a rate of 70,000 axial scans/sec with a scan angle of up to 40°×40° was recently introduced, providing large-field images. Tested on 10 eyes from 5 healthy subjects, the system has been shown to provide reproducible images.[87]

Another group designed a swept source PS-OCT (SS-PS-OCT) device with a 1059 nm wavelength light source and an axial scan rate of 34,000 axial scans/sec.[88] The authors reported that RNFL phase retardation measurements acquired with their system compared well with those acquired using a commercial scanning laser polarimetry instrument.

A new method to correct system polarization distortions and further improve PS-OCT images was recently introduced.[89] The correction of system polarization distortions yielded reduced phase retardation noise, and better estimates of the diattenuation and the relative optic axis orientation in weakly birefringent tissues.

The SS-PS-OCT device was also used to scan the anterior segment in 31 healthy subjects in order to assess the visibility of the trabecular meshwork.[90] Three independent graders compared a total of 496 standard scattering OCT and phase-retardation tomography images that were obtained simultaneously. The results demonstrated statistically significant improvement of visibility in the PS-OCT images compared with conventional OCT images that can improve the assessment of the anterior chamber angle in clinical practice.

While this technology offers several unique perspectives for assessing retinal integrity and functionality, the role of this technology in clinical management of glaucoma patients is still under investigation.

OCT Blood Flow

A different approach to using the information provided by OCT technology to assess the functional tissue status is to examine the blood flow characteristics. [Figure 7] Previous studies have demonstrated that ONH blood flow is compromised in glaucoma patients, thus the estimation of tissue perfusion alterations might help in glaucoma diagnosis.

Nineteen eyes of subjects with perimetric glaucoma were examined with Doppler SD-OCT.[91] The average retinal blood flow and arterial and venous velocities were significantly lower in the preperimetric eyes than in healthy eyes. The decrease in blood flow was correlated with VF mean deviation. A study of 27 healthy eyes and 30 eyes with hemifield VF defects used Doppler SD-OCT to evaluate total and hemispheric retinal blood flow.[92] Glaucomatous eyes showed reduced total retinal blood flow and venous cross-sectional area when compared with healthy eyes. The reduction in retinal blood flow was correlated with VF, circumpapillary RNFL, and macular ganglion cell complex thinning. Moreover, the retinal blood flow reduction and the thinning of the RNFL and the ganglion cell complex were also observed in the apparently normal visual hemifield, which might indicate it to be a sensitive tool for detecting early disease.

ONH blood flow was assessed in glaucomatous and healthy eyes using a new method for data processing.[**77] The optic disc microcirculation was examined in 24 healthy and 11 glaucoma subjects using a high-speed 1050 nm wavelength SS-OCT and split-spectrum

amplitude-decorrelation angiography (SSADA) algorithm to compute 3D optic disc angiography. The blood flow is assessed by calculating the laser beam signal amplitude decorrelation from consecutive cross-section scans. The contrast image that distinguishes the static and moving tissue is able to visualize the blood flow. The decorrelation is proportional to the red blood cells flow speed across the laser beam. This information is used to calculate blood flow velocity. The results demonstrated good intra-visit repeatability (coefficient of variance = 1.2%) and inter-visit reproducibility (coefficient of variance = 4.2%). The disc flow index was 25% lower in the glaucoma group ($P = 0.003$) compared with the healthy group, and it was strongly correlated ($R^2 = 0.752$) with VF pattern standard deviation.

OCT Aqueous Humor Outflow

OCT technique is capable of noninvasively imaging the primary aqueous humor outflow system in living human eyes.[93],[94] The authors characterized the pattern of Schlemm's canal, demonstrating the marked size variability along the canal and the 3D path of the outflow system.[95],[*96] The temporal limbus area of healthy subjects was scanned with SD-OCT while elevating IOP by the application of an ophthalmodynamometer. The results demonstrated a significant reduction in Schlemm's canal cross-sectional area with acute IOP elevation.[97] This acute response to pressure elevation might be useful in determining eyes at risk for impaired outflow drainage. The ability to gather in-vivo information on the outflow pathway might improve understanding of glaucoma pathogenesis, assist in glaucoma surgical planning, and aid in clinical management.

Phase-sensitive OCT

Phase-sensitive OCT is a new development in OCT capable of imaging cellular scale tissue vibrations. The OCT signal typically encodes both the intensity and the phase of the reflection from the scanned region. Minute tissue movements alter the phase of light reflected back to the OCT system, which is normally ignored in conventional OCT. These phase changes can be detected by phase-sensitive OCT and used to characterize physiologic movements as small as 0.26nm.[98] Because this system is so sensitive to minute motion, most studies using this system were performed ex-vivo. However, phase-sensitive OCT offers the advantage of not only assessing the structure of tissue, but also its function.

Cardiac pulse-induced motion of trabecular meshwork (TM) has been quantitatively assessed in healthy living eyes using phase-sensitive OCT.[99] This method has the ability to better characterize TM biomechanical properties responsible for ocular outflow regulation. The understanding of aqueous outflow regulation and the alteration of regulatory mechanism in glaucoma may lead to development of new diagnostic and treatment procedures. Phase-sensitive OCT has also been shown to allow precise quantification of the length changes in the outer segment of the photoreceptors over the span of a few hours.[100]

Summary

The ocular imaging field is in the midst of a very active stage of technological enhancements through the evolvement of innovative technology and image processing methods that further enhance disease detection and monitoring. These advancements will improve our

understanding of the glaucomatous process, improve the ability to detect the disease at the earliest stages, and allow precise monitoring of disease behavior over time so that clinicians can optimize treatment of glaucoma patients and preserve functional vision.

Acknowledgements

Supported in part by National Institutes of Health contracts R01-EY013178, P30-EY008098 (Bethesda, MD); Eye and Ear Foundation (Pittsburgh, PA); Research to Prevent Blindness (New York, NY).

References

Papers of special note have been highlighted as:

* of interest

** of considerable interest

1. Friedman DS, Wolfs RCW, O'Colmain BJ, et al. Prevalence of open-angle glaucoma among adults in the United States. Arch. Ophthalmol. 2004; 122:532–538. [PubMed: 15078671]
2. Huang D, Swanson EA, Lin CP, et al. Optical coherence tomography. Science. 1991; 254:1178–1181. [PubMed: 1957169]
3. Hee MR, Izatt JA, Swanson EA, et al. Optical coherence tomography of the human retina. Arch. Ophthalmol. 1995; 113:325–332. [PubMed: 7887846]
4. Fercher AF, Hitzenberger CK, Drexler W, et al. In vivo optical coherence tomography. Am. J. Ophthalmol. 1993; 116:113–114. [PubMed: 8328536]
5. Wojtkowski, M.; Fercher, AF.; Leitgeb, R. [[cited 2014 Sep 6]] Phase-sensitive interferometry in optical coherence tomography. 2001. p. 250-255.Available from: http://dx.doi.org/10.1117/12.432985
6. Wieser W, Biedermann BR, Klein T, et al. Multi-megahertz OCT: High quality 3D imaging at 20 million A-scans and 4.5 GVoxels per second. Opt. Express. 2010; 18:14685–14704. [PubMed: 20639955]
7. Schuman JS. Spectral domain optical coherence tomography for glaucoma (an AOS thesis). Trans. Am. Ophthalmol. Soc. 2008; 106:426–458. [PubMed: 19277249]
8. Menke MN, Knecht P, Sturm V, et al. Reproducibility of Nerve Fiber Layer Thickness Measurements Using 3D Fourier-Domain OCT. Invest. Ophthalmol. Vis. Sci. 2008; 49:5386–5391. [PubMed: 18676630]
9. Garas A, Vargha P, Holló G. Reproducibility of retinal nerve fiber layer and macular thickness measurement with the RTVue-100 optical coherence tomograph. Ophthalmology. 2010; 117:738–746. [PubMed: 20079538]
10. Mwanza J-C, Chang RT, Budenz DL, et al. Reproducibility of peripapillary retinal nerve fiber layer thickness and optic nerve head parameters measured with cirrus HD-OCT in glaucomatous eyes. Invest. Ophthalmol. Vis. Sci. 2010; 51:5724–5730. [PubMed: 20574014]
11. Mansouri K, Leite MT, Medeiros FA, et al. Assessment of rates of structural change in glaucoma using imaging technologies. Eye. 2011; 25:269–277. [PubMed: 21212798]
12. Leung CKS, Lam S, Weinreb RN, et al. Retinal nerve fiber layer imaging with spectral-domain optical coherence tomography: analysis of the retinal nerve fiber layer map for glaucoma detection. Ophthalmology. 2010; 117:1684–1691. [PubMed: 20663563]
13. Mwanza J-C, Oakley JD, Budenz DL, et al. Ability of cirrus HD-OCT optic nerve head parameters to discriminate normal from glaucomatous eyes. Ophthalmology. 2011; 118:241–248.e1. [PubMed: 20920824]
14. Moreno PAM, Konno B, Lima VC, et al. Spectral-domain optical coherence tomography for early glaucoma assessment: analysis of macular ganglion cell complex versus peripapillary retinal nerve fiber layer. Can. J. Ophthalmol. J. Can. Ophtalmol. 2011; 46:543–547.

15. Nakatani Y, Higashide T, Ohkubo S, et al. Evaluation of macular thickness and peripapillary retinal nerve fiber layer thickness for detection of early glaucoma using spectral domain optical coherence tomography. J. Glaucoma. 2011; 20:252–259. [PubMed: 20520570]

16. Huang J-Y, Pekmezci M, Mesiwala N, et al. Diagnostic power of optic disc morphology, peripapillary retinal nerve fiber layer thickness, and macular inner retinal layer thickness in glaucoma diagnosis with fourier-domain optical coherence tomography. J. Glaucoma. 2011; 20:87–94. [PubMed: 20577117]

17. Kang SY, Sung KR, Na JH, et al. Comparison between deviation map algorithm and peripapillary retinal nerve fiber layer measurements using Cirrus HD-OCT in the detection of localized glaucomatous visual field defects. J. Glaucoma. 2012; 21:372–378. [PubMed: 21430549]

18. Kotowski J, Folio LS, Wollstein G, et al. Glaucoma Discrimination of Segmented Cirrus Spectral Domain Optical Coherence Tomography (SD-OCT) Macular Scans. Br. J. Ophthalmol. 2012; 96:1420–1425. [PubMed: 22914498]

19. Lisboa R, Leite MT, Zangwill LM, et al. Diagnosing Preperimetric Glaucoma with Spectral Domain Optical Coherence Tomography. Ophthalmology. 2012; 119:2261–2269. [PubMed: 22883689]

20. Sehi M, Grewal DS, Sheets CW, Greenfield DS. Diagnostic Ability of Fourier-Domain Versus Time-Domain Optical Coherence Tomography for Glaucoma Detection. Am. J. Ophthalmol. 2009; 148:597–605. [PubMed: 19589493]

21. Jeoung JW, Park KH. Comparison of Cirrus OCT and Stratus OCT on the ability to detect localized retinal nerve fiber layer defects in preperimetric glaucoma. Invest. Ophthalmol. Vis. Sci. 2010; 51:938–945. [PubMed: 19797208]

22. Choi SS, Zawadzki RJ, Lim MC, et al. Evidence of outer retinal changes in glaucoma patients as revealed by ultrahigh-resolution in vivo retinal imaging. Br. J. Ophthalmol. 2011; 95:131–141. [PubMed: 20956277] * The study demonstrated structural changes in cone photoreceptors in glaucomatous eyes using AO technology in vivo

23. Aref AA, Budenz DL. Spectral domain optical coherence tomography in the diagnosis and management of glaucoma. Ophthalmic Surg. Lasers Imaging Off. J. Int. Soc. Imaging Eye. 2010; (41 Suppl):S15–S27.

24. Schuman JS, Hee MR, Puliafito CA, et al. Quantification of nerve fiber layer thickness in normal and glaucomatous eyes using optical coherence tomography. Arch. Ophthalmol. 1995; 113:586–596. [PubMed: 7748128]

25. Gabriele ML, Ishikawa H, Wollstein G, et al. Optical coherence tomography scan circle location and mean retinal nerve fiber layer measurement variability. Invest. Ophthalmol. Vis. Sci. 2008; 49:2315–2321. [PubMed: 18515577]

26. Leung CK-S, Cheung CY-L, Weinreb RN, et al. Retinal nerve fiber layer imaging with spectral-domain optical coherence tomography: a variability and diagnostic performance study. Ophthalmology. 2009; 116:1257–1263. 1263.e1–1263.e2. [PubMed: 19464061]

27. Alasil T, Wang K, Keane PA, et al. Analysis of normal retinal nerve fiber layer thickness by age, sex, and race using spectral domain optical coherence tomography. J. Glaucoma. 2013; 22:532–541. [PubMed: 22549477]

28. Hong S, Kim CY, Lee WS, Seong GJ. Reproducibility of peripapillary retinal nerve fiber layer thickness with spectral domain cirrus high-definition optical coherence tomography in normal eyes. Jpn. J. Ophthalmol. 2010; 54:43–47. [PubMed: 20151275]

29. Carpineto P, Nubile M, Agnifili L, et al. Reproducibility, repeatability of Cirrus™ HD-OCT peripapillary retinal nerve fibre layer thickness measurements in young normal subjects. Ophthalmol. J. Int. Ophtalmol. Int. J. Ophthalmol. Z. Für Augenheilkd. 2012; 227:139–145.

30. Töteberg-Harms M, Sturm V, Knecht PB, Funk J, Menke MN. Repeatability of nerve fiber layer thickness measurements in patients with glaucoma and without glaucoma using spectral-domain and time-domain OCT. Graefes Arch. Clin. Exp. Ophthalmol. Albrecht Von Graefes Arch. Für Klin. Exp. Ophthalmol. 2012; 250:279–287.

31. Bendschneider D, Tornow RP, Horn FK, et al. Retinal nerve fiber layer thickness in normals measured by spectral domain OCT. J. Glaucoma. 2010; 19:475–482. [PubMed: 20051888]
32. Celebi ARC, Mirza GE. Age-related change in retinal nerve fiber layer thickness measured with spectral domain optical coherence tomography. Invest. Ophthalmol. Vis. Sci. 2013; 54:8095–8103. [PubMed: 24194190]
33. Leite MT, Rao HL, Zangwill LM, et al. Comparison of the diagnostic accuracies of the Spectralis, Cirrus, and RTVue optical coherence tomography devices in glaucoma. Ophthalmology. 2011; 118:1334–1339. [PubMed: 21377735]
34. Tan BB, Natividad M, Chua K-C, Yip LWMbc. Comparison of Retinal Nerve Fiber Layer Measurement Between 2 Spectral Domain OCT Instruments. J. Glaucoma April. 2012; 21:266–273.
35. Bengtsson B, Andersson S, Heijl A. Performance of time-domain and spectral-domain Optical Coherence Tomography for glaucoma screening. Acta Ophthalmol. 2012; 90:310–315. [PubMed: 20946342]
36. Kim NR, Lee ES, Seong GJ, et al. Spectral-domain optical coherence tomography for detection of localized retinal nerve fiber layer defects in patients with open-angle glaucoma. Arch. Ophthalmol. 2010; 128:1121–1128. [PubMed: 20837794]
37. He L, Ren R, Yang H, Anatomic vs, et al. Acquired Image Frame Discordance in Spectral Domain Optical Coherence Tomography Minimum Rim Measurements. PLoS ONE. 2014; 9:e92225. [PubMed: 24643069]
38. Savini G, Carbonelli M, Parisi V, Barboni P. Repeatability of optic nerve head parameters measured by spectral-domain OCT in healthy eyes. Ophthalmic Surg. Lasers Imaging Off. J. Int. Soc. Imaging Eye. 2011; 42:209–215.
39. Kratz A, Lim R, Goldberg I. Optic nerve head assessment: comparison of Cirrus optic coherence tomography and Heidelberg Retinal Tomograph 3 Clin. Experiment. Ophthalmol. 2014; 42:734–744.
40. Cheung CY, Chen D, Wong TY, et al. Determinants of quantitative optic nerve measurements using spectral domain optical coherence tomography in a population-based sample of non-glaucomatous subjects. Invest. Ophthalmol. Vis. Sci. 2011; 52:9629–9635. [PubMed: 22039236]
41. Girkin CA, McGwin G, Sinai MJ, et al. Variation in optic nerve and macular structure with age and race with spectral-domain optical coherence tomography. Ophthalmology. 2011; 118:2403–2408. [PubMed: 21907415]
42. Kim NR, Kim JH, Kim CY, et al. Comparison of the optic nerve imaging by time-domain optical coherence tomography and Fourier-domain optical coherence tomography in distinguishing normal eyes from those with glaucoma. J. Glaucoma. 2013; 22:36–43. [PubMed: 21623218]
43. Rao HL, Zangwill LM, Weinreb RN, et al. Comparison of Different Spectral Domain Optical Coherence Tomography Scanning Areas for Glaucoma Diagnosis. Ophthalmology. 2010; 117:1692–1699.e1. [PubMed: 20493529]
44. Sung KR, Na JH, Lee Y. Glaucoma diagnostic capabilities of optic nerve head parameters as determined by Cirrus HD optical coherence tomography. J. Glaucoma. 2012; 21:498–504. [PubMed: 21637115]
45. Chauhan BC, O'Leary N, AlMobarak FA, et al. Enhanced Detection of Open-angle Glaucoma with an Anatomically Accurate Optical Coherence Tomography-Derived Neuroretinal Rim Parameter. Ophthalmology. 2013; 120:535–543. [PubMed: 23265804]
46. Curcio CA, Allen KA. Topography of ganglion cells in human retina. J. Comp. Neurol. 1990; 300:5–25. [PubMed: 2229487]
47. Ishikawa H, Stein DM, Wollstein G, et al. Macular Segmentation with Optical Coherence Tomography. Invest. Ophthalmol. Vis. Sci. 2005; 46:2012–2017. [PubMed: 15914617]
48. Tan O, Li G, Lu AT-H, et al. Advanced Imaging for Glaucoma Study Group. Mapping of macular substructures with optical coherence tomography for glaucoma diagnosis. Ophthalmology. 2008; 115:949–956. [PubMed: 17981334]
49. Nakano N, Hangai M, Nakanishi H, et al. Macular ganglion cell layer imaging in preperimetric glaucoma with speckle noise-reduced spectral domain optical coherence tomography. Ophthalmology. 2011; 118:2414–2426. [PubMed: 21924499]

50. Ooto S, Hangai M, Tomidokoro A, et al. Effects of age, sex, and axial length on the three-dimensional profile of normal macular layer structures. Invest. Ophthalmol. Vis. Sci. 2011; 52:8769–8779. [PubMed: 21989721]

51. Takayama K, Hangai M, Durbin M, et al. A novel method to detect local ganglion cell loss in early glaucoma using spectral-domain optical coherence tomography. Invest. Ophthalmol. Vis. Sci. 2012; 53:6904–6913. [PubMed: 22977136]

52. Bussel II, Wollstein G, Schuman JS. OCT for glaucoma diagnosis, screening and detection of glaucoma progression. Br. J. Ophthalmol. 2013 bjophthalmol - 2013- 304326.

53. Francoz M, Fenolland J-R, Giraud J-M, et al. Reproducibility of macular ganglion cell-inner plexiform layer thickness measurement with cirrus HD-OCT in normal, hypertensive and glaucomatous eyes. Br. J. Ophthalmol. 2014; 98:322–328. [PubMed: 24307717]

54. Mwanza J-C, Durbin MK, Budenz DL, et al. Glaucoma diagnostic accuracy of ganglion cell-inner plexiform layer thickness: comparison with nerve fiber layer and optic nerve head. Ophthalmology. 2012; 119:1151–1158. [PubMed: 22365056]

55. Jeoung JW, Choi YJ, Park KH, Kim DM. Macular ganglion cell imaging study: glaucoma diagnostic accuracy of spectral-domain optical coherence tomography. Invest. Ophthalmol. Vis. Sci. 2013; 54:4422–4429. [PubMed: 23722389]

56. Seo JH, Kim T-W, Weinreb RN, et al. Detection of Localized Retinal Nerve Fiber Layer Defects with Posterior Pole Asymmetry Analysis of Spectral Domain Optical Coherence Tomography. Invest. Ophthalmol. Vis. Sci. 2012; 53:4347–4353. [PubMed: 22577076]

57. Liu B, Brezinski ME. Theoretical and practical considerations on detection performance of time domain, Fourier domain, and swept source optical coherence tomography. J. Biomed. Opt. 2007; 12:044007. [PubMed: 17867811]

58. Potsaid B, Baumann B, Huang D, et al. Ultrahigh speed 1050nm swept source/Fourier domain OCT retinal and anterior segment imaging at 100,000 to 400,000 axial scans per second. Opt. Express. 2010; 18:20029–20048. [PubMed: 20940894]

59. Regatieri CV, Branchini L, Fujimoto JG, Duker JS. CHOROIDAL IMAGING USING SPECTRAL-DOMAIN OPTICAL COHERENCE TOMOGRAPHY. Retina Phila. Pa. 2012; 32:865–876.

60. Kagemann L, Ishikawa H, et al. Wollstein G Ultrahigh-resolution Spectral Domain Optical Coherence Tomography Imaging of the Lamina Cribrosa. Ophthalmic Surg. Lasers Imaging Off. J. Int. Soc. Imaging Eye. 2008; 39:S126–S131.

61. Park H-YL, Jeon SH, Park CK. Enhanced Depth Imaging Detects Lamina Cribrosa Thickness Differences in Normal Tension Glaucoma and Primary Open-Angle Glaucoma. Ophthalmology. 2012; 119:10–20. [PubMed: 22015382]

62. Adhi M, Liu JJ, Qavi AH, et al. Enhanced visualization of the choroido-scleral interface using swept-source OCT. Ophthalmic Surg. Lasers Imaging Retina. 2013; 44:S40–S42. [PubMed: 24220884]

63. Copete S, Flores-Moreno I, Montero JA, et al. Direct comparison of spectral-domain and swept-source OCT in the measurement of choroidal thickness in normal eyes. Br. J. Ophthalmol. 2014; 98:334–338. [PubMed: 24288394]

64. Takayama K, Hangai M, Kimura Y, et al. Three-dimensional imaging of lamina cribrosa defects in glaucoma using swept-source optical coherence tomography. Invest. Ophthalmol. Vis. Sci. 2013; 54:4798–4807. [PubMed: 23778878] * Strong association of full-thickness LC defects with localized glaucomatous damage was observed using in vivo SS-OCT imaging

65. Wang B, Nevins JE, Nadler Z, et al. In vivo lamina cribrosa micro-architecture in healthy and glaucomatous eyes as assessed by optical coherence tomography. Invest. Ophthalmol. Vis. Sci. 2013; 54:8270–8274. [PubMed: 24302585] ** Changes in the LC micro-architecture in eyes with glaucoma were assessed in vivo using SS-OCT

66. McKee H, Ye C, Yu M, et al. Anterior chamber angle imaging with swept-source optical coherence tomography: detecting the scleral spur, Schwalbe's Line, and Schlemm's Canal. J. Glaucoma. 2013; 22:468–472. [PubMed: 23377578]

67. Lopilly Park H-Y, Lee NY, Choi JA, Park CK. Measurement of scleral thickness using swept-source optical coherence tomography in patients with open-angle glaucoma and myopia. Am. J. Ophthalmol. 2014; 157:876–884. [PubMed: 24412142]

68. Mansouri K, Medeiros FA, Tatham AJ, et al. Evaluation of retinal and choroidal thickness by swept-source optical coherence tomography: repeatability and assessment of artifacts. Am. J. Ophthalmol. 2014; 157:1022–1032. [PubMed: 24531020]

69. Nadler Z, Wang B, Wollstein G, et al. Automated lamina cribrosa microstructural segmentation in optical coherence tomography scans of healthy and glaucomatous eyes. Biomed. Opt. Express. 2013; 4:2596–2608. [PubMed: 24298418]

70. Yoshikawa M, Akagi T, Hangai M, et al. Alterations in the neural and connective tissue components of glaucomatous cupping after glaucoma surgery using swept-source optical coherence tomography. Invest. Ophthalmol. Vis. Sci. 2014; 55:477–484. [PubMed: 24398100]

71. Lai I, Mak H, Lai G, et al. Anterior chamber angle imaging with swept-source optical coherence tomography: measuring peripheral anterior synechia in glaucoma. Ophthalmology. 2013; 120:1144–1149. [PubMed: 23522970]

72. Mishima K, Tomidokoro A, Suramethakul P, et al. Iridotrabecular contact observed using anterior segment three-dimensional OCT in eyes with a shallow peripheral anterior chamber. Invest. Ophthalmol. Vis. Sci. 2013; 54:4628–4635. [PubMed: 23761081]

73. Tun TA, Baskaran M, Zheng C, et al. Assessment of trabecular meshwork width using swept source optical coherence tomography. Graefes Arch. Clin. Exp Ophthalmol. Albrecht Von Graefes Arch. Für Klin. Exp. Ophthalmol. 2013; 251:1587–1592.

74. Ho S-W, Baskaran M, Zheng C, et al. Swept source optical coherence tomography measurement of the iris-trabecular contact (ITC) index: a new parameter for angle closure. Graefes Arch. Clin. Exp Ophthalmol. Albrecht Von Graefes ArchFür Klin. Exp. Ophthalmol. 2013; 251:1205–1211.

75. Baskaran M, Ho S-W, Tun TA, et al. Assessment of Circumferential Angle-Closure by the Iris-Trabecular Contact Index with Swept-Source Optical Coherence Tomography. Ophthalmology. 2013; 120:2226–2231. [PubMed: 23774103]

76. Ni, Ni S.; Tian, J.; Marziliano, P.; Wong, H-T. Anterior Chamber Angle Shape Analysis and Classification of Glaucoma in SS-OCT Images. J. Ophthalmol. 2014; 2014:942367. [PubMed: 25197561]

77. Jia Y, Wei E, Wang X, et al. Optical Coherence Tomography Angiography of Optic Disc Perfusion in Glaucoma. Ophthalmology. 2014; 121:1322–1332. [PubMed: 24629312] ** OCT shows the ability to assess optic disc perfusion changes in glaucoma in non-invasive way without injecting a dye

78. Xue B, Choi SS, Doble N, Werner JS. Photoreceptor counting and montaging of en-face retinal images from an adaptive optics fundus camera. J. Opt. Soc. Am. A Opt. Image Sci. Vis. 2007; 24:1364–1372. [PubMed: 17429482]

79. Prasse M, Rauscher FG, Wiedemann P, et al. Optical properties of retinal tissue and the potential of adaptive optics to visualize retinal ganglion cells in vivo. Cell Tissue Res. 2013; 353:269–278. [PubMed: 23529360]

80. Takayama K, Ooto S, Hangai M, et al. High-resolution imaging of retinal nerve fiber bundles in glaucoma using adaptive optics scanning laser ophthalmoscopy. Am. J. Ophthalmol. 2013; 155:870–881. [PubMed: 23352341]

81. Werner JS, Keltner JL, Zawadzki RJ, Choi SS. Outer retinal abnormalities associated with inner retinal pathology in nonglaucomatous and glaucomatous optic neuropathies. Eye. 2011; 25:279–289. [PubMed: 21293495]

82. Kocaoglu OP, Cense B, Jonnal RS, et al. Imaging retinal nerve fiber bundles using optical coherence tomography with adaptive optics. Vision Res. 2011; 51:1835–1844. [PubMed: 21722662] *

Changes in individual retinal nerve fiber's width in glaucomatous eyes were detected by AO scanning laser ophthalmoscopy

83. Nadler Z, Wang B, Wollstein G, et al. Repeatability of in vivo 3D lamina cribrosa microarchitecture using adaptive optics spectral domain optical coherence tomography. Biomed. Opt. Express. 2014; 5:1114–1123. [PubMed: 24761293]
84. Gotzinger E, Pircher M, Baumann B, et al. Three-dimensional polarization sensitive OCT imaging and interactive display of the human retina. Opt. Express. 2009; 17:4151–4165. [PubMed: 19259252]
85. Yamanari M, Makita S, Lim Y, Yasuno Y. Full-range polarization-sensitive swept-source optical coherence tomography by simultaneous transversal and spectral modulation. Opt. Express. 2010; 18:13964–13980. [PubMed: 20588529]
86. Cense B, Koperda E, Brown JM, et al. Volumetric retinal imaging with ultrahigh-resolution spectral-domain optical coherence tomography and adaptive optics using two broadband light sources. Opt. Express. 2009; 17:4095–4111. [PubMed: 19259249]
87. Zotter S, Pircher M, Götzinger E, et al. Measuring retinal nerve fiber layer birefringence, retardation, and thickness using wide-field, high-speed polarization sensitive spectral domain OCT. Invest. Ophthalmol. Vis. Sci. 2013; 54:72–84. [PubMed: 23221076]
88. Elmaanaoui B, Wang B, Dwelle JC, et al. Birefringence measurement of the retinal nerve fiber layer by swept source polarization sensitive optical coherence tomography. Opt. Express. 2011; 19:10252–10268. [PubMed: 21643283]
89. Braaf B, Vermeer KA, de Groot M, et al. Fiber-based polarization-sensitive OCT of the human retina with correction of system polarization distortions. Biomed. Opt. Express. 2014; 5:2736–2758. [PubMed: 25136498]
90. Yasuno Y, Yamanari M, Kawana K, et al. Visibility of trabecular meshwork by standard and polarization-sensitive optical coherence tomography. J. Biomed. Opt. 2010; 15 061705-061705-10.
91. Wang Y, Fawzi AA, Varma R, et al. Pilot Study of Optical Coherence Tomography Measurement of Retinal Blood Flow in Retinal and Optic Nerve Diseases. Invest. Ophthalmol. Vis. Sci. 2011; 52:840–845. [PubMed: 21051715]
92. Sehi M, Goharian I, Konduru R, et al. Retinal blood flow in glaucomatous eyes with single-hemifield damage. Ophthalmology. 2014; 121:750–758. [PubMed: 24290800]
93. Kagemann L, Wollstein G, Ishikawa H, et al. Identification and assessment of Schlemm's canal by spectral-domain optical coherence tomography. Invest. Ophthalmol. Vis. Sci. 2010; 51:4054–4059. [PubMed: 20237244]
94. Francis AW, Kagemann L, Wollstein G, et al. Morphometric analysis of aqueous humor outflow structures with spectral-domain optical coherence tomography. Invest. Ophthalmol. Vis. Sci. 2012; 53:5198–5207. [PubMed: 22499987]
95. Kagemann L, Wollstein G, Ishikawa H, et al. 3D visualization of aqueous humor outflow structures in-situ in humans. Exp. Eye Res. 2011; 93:308–315. [PubMed: 21514296]
96. Kagemann L, Nevins JE, Jan N-J, et al. Characterisation of Schlemm's canal cross-sectional area. Br. J. Ophthalmol. 2014; 98(Suppl 2):i10–i14. * The effect effect of acute increase of IOP on Schlemm's canal cross-sectional area was evaluated in vivo with SD-OCT in human eyes
97. Kagemann L, Wang B, Wollstein G, et al. IOP Elevation Reduces Schlemm's Canal Cross-Sectional Area. Invest. Ophthalmol. Vis. Sci. 2014; 55:1805–1809. [PubMed: 24526436]
98. Wang RK, Kirkpatrick S, Hinds M. Phase-sensitive optical coherence elastography for mapping tissue microstrains in real time. Appl. Phys. Lett. 2007; 90:164105.
99. Li P, Shen TT, Johnstone M, Wang RK. Pulsatile motion of the trabecular meshwork in healthy human subjects quantified by phase-sensitive optical coherence tomography. Biomed. Opt. Express. 2013; 4:2051–2065. [PubMed: 24156063]
100. Jonnal RS, Kocaoglu OP, Wang Q, et al. Phase-sensitive imaging of the outer retina using optical coherence tomography and adaptive optics. Biomed. Opt. Exp. 2012; 3:104–124.

Expert commentary

OCT technology transforms the way glaucoma is diagnosed and monitored by providing reliable structural and functional information on ocular tissues vulnerable to glaucomatous damage. The continuous evolution of the technology results in substantial increase in scanning speed, better visualization of tissue microstructure and ability to assess functional aspects of ocular structures. Implementation of these improvements in eye imaging enables the assessment of subtle glaucomatous structural and functional changes thus enhancing diagnosis and disease progression detection.

Five-year view

Considering the rapid and continuous developments it is difficult to predict the status of OCT technology even in near future. The ongoing research is mostly focused on further increase in OCT scanning speed, scanning resolutions, penetration depth and improvements in image registration and processing software. The incorporation of functional analysis will allow an automated and objective assessment of the glaucomatous damage offering a new clinical diagnostic tool. The rapid evolvement of the OCT technology ensures that excellent diagnostic tool will be available clinically to further improve glaucoma management.

Key Issues

- The improved specifications of ocular imaging allow better disease diagnosis and monitoring capabilities and further insight into the pathophysiology of glaucoma.
- Spectral-domain OCT technology uses the light frequency information to determine the spatial location of reflected light and to provide in vivo high-resolution images.
- Swept-source OCT (SS-OCT) acquires frequency information by sweeping a narrow bandwidth light source through a broad range of frequencies.
- Adaptive optics (AO) method corrects optical aberrations and when coupled with ocular imaging devices can provide in-vivo images of the retinal microvasculature, photoreceptors, ganglion cells, and the lamina cribrosa at the cellular level.
- Polarization sensitive OCT provides cross-sectional intensity information with the polarization status of the tissue.
- Phase-sensitive OCT enables detection of minute, sub-cellular level movements.

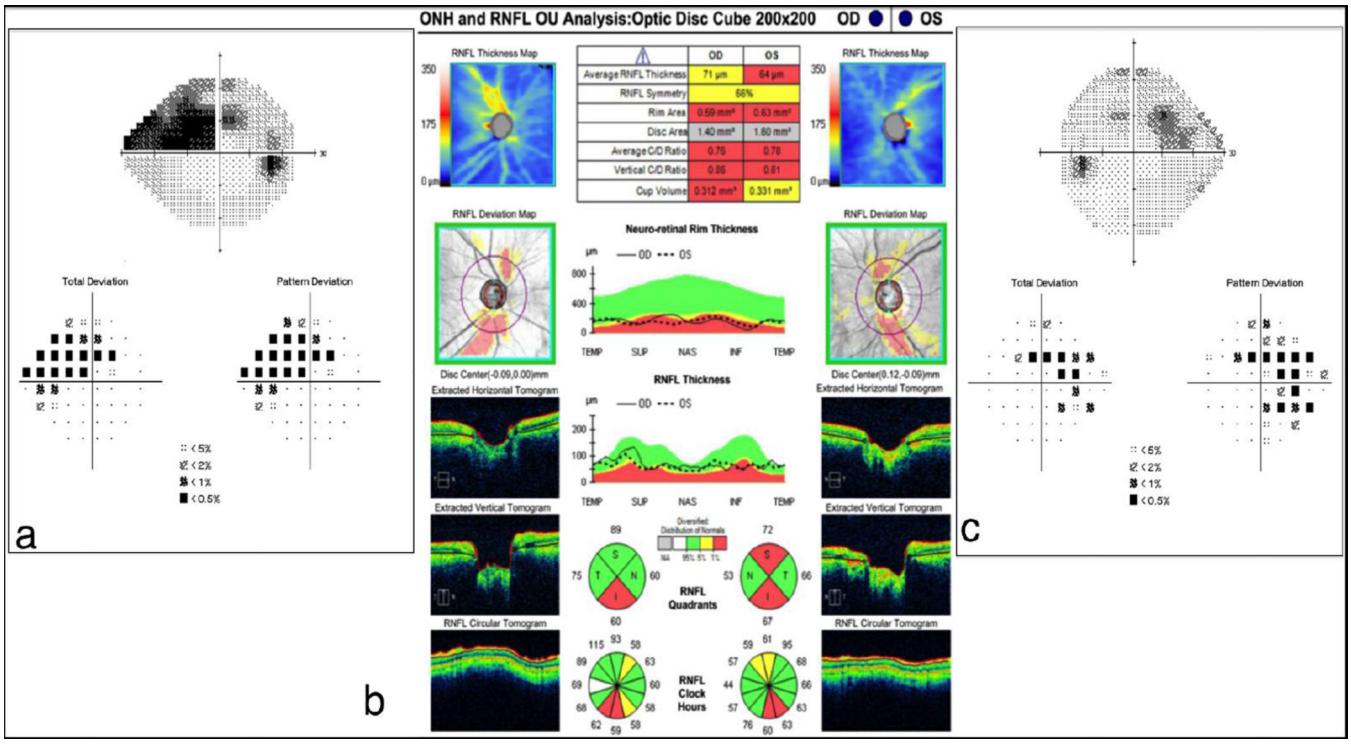

Figure 1. Cirrus HD-OCT ONH and RNFL Analysis

Significant RNFL thinning (red) is seen in the inferior quadrants of both eyes and in the superior quadrants of the left eye (b). Visual field defects are noted in the correspondent areas (a and c).

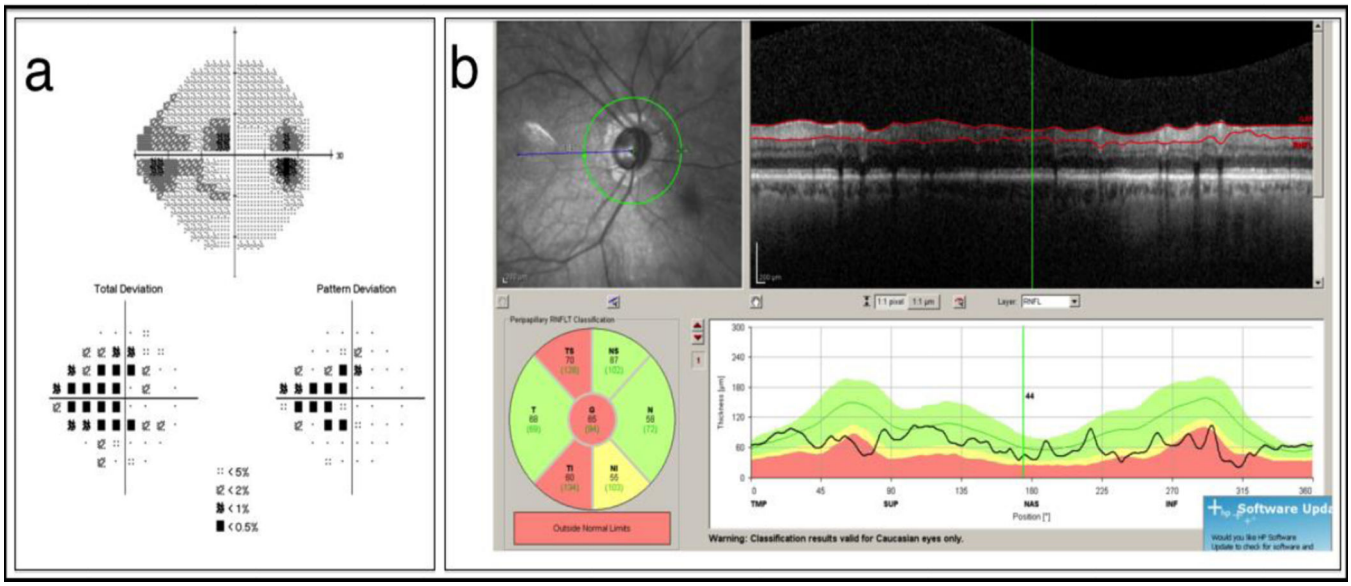

Figure 2. Spectralis OCT RNFL Analysis

Significant RNFL thinning (red) is detected in the inferotemporal and superotemporal sectors (b). Visual field defects are noted in the correspondent sectors (a).

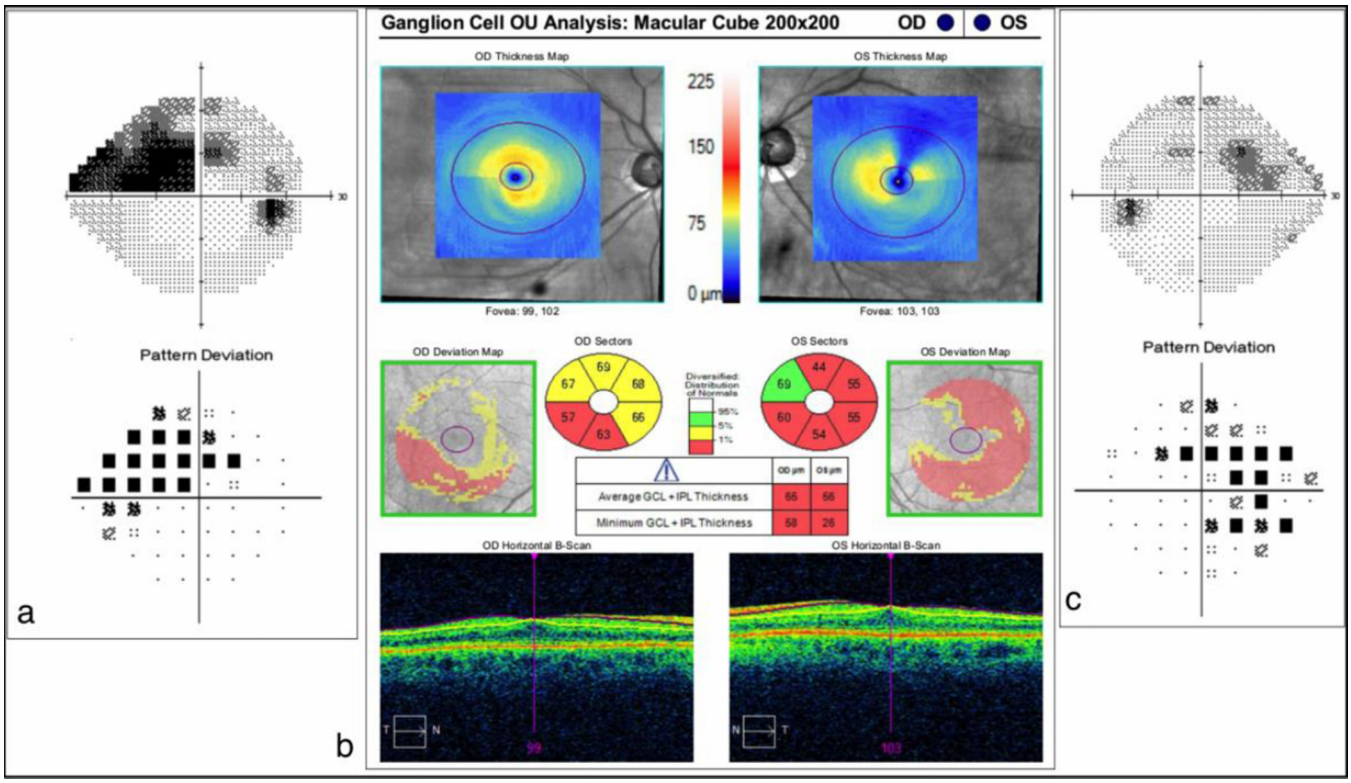

Figure 3. Cirrus HD-OCT Ganglion Cell Analysis

Significant ganglion cell and inner plexiform layers thinning (red) is seen on the thickness, sectoral and deviation maps in both eyes (b). Visual field defects are noted in the correspondent areas (a and c).

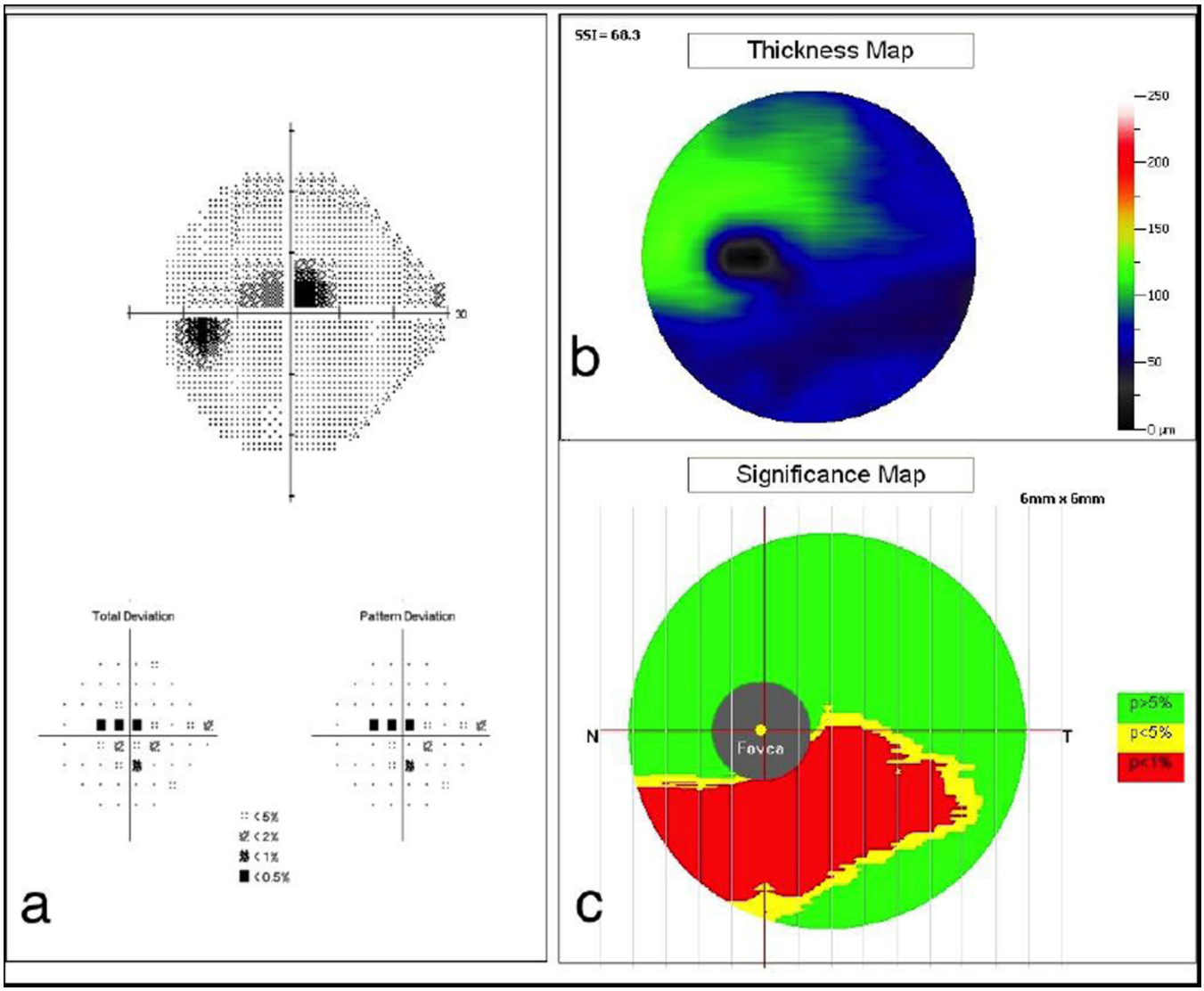

Figure 4. RTVue Premier Gangion Cell Complex Analysis

Significant ganglion cell complex thinning (red) is seen in the inferior macular area (b and c) with the correspondent superior central visual field defect (a).

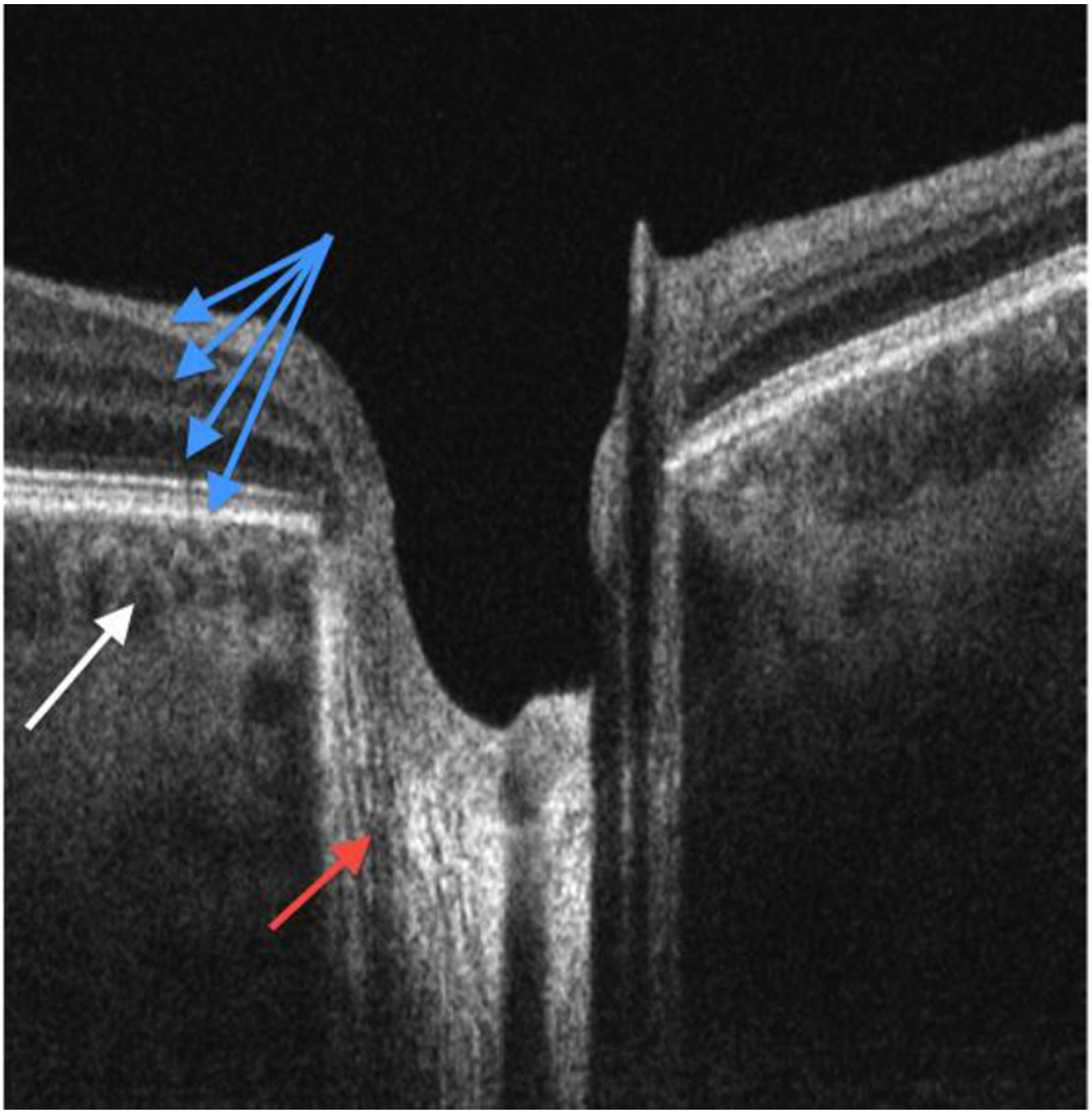

Figure 5.

Swept-source OCT cross section. The retinal layers (blue arrows), nerve fiber fascicles passing through lamina cribrosa (red arrow) and choroidal vessels (white arrow) are all visualized in the same scan because this technology is less affected by signal drop-off in comparison with other OCT iterations.

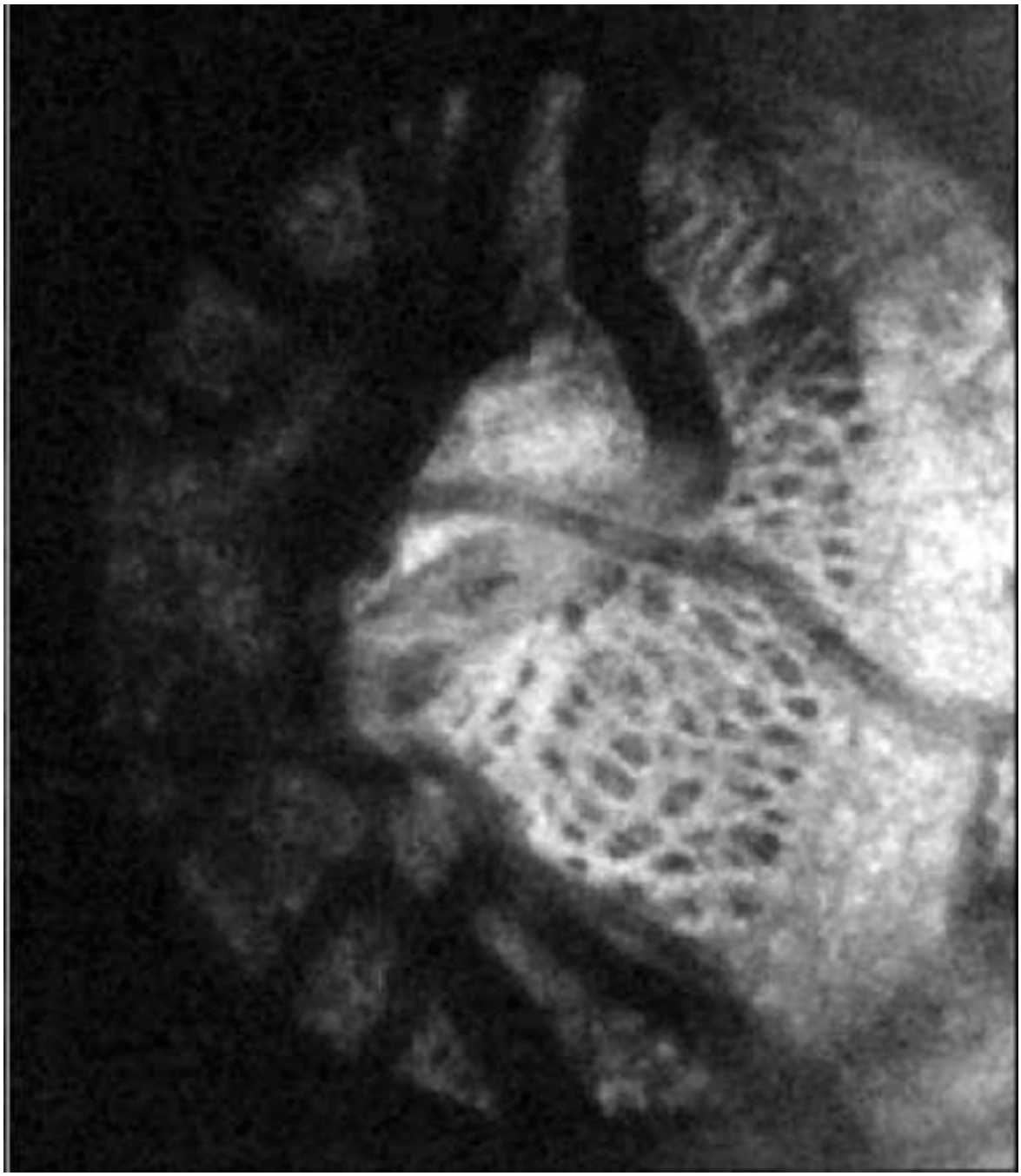

Figure 6.
Adaptive optics OCT en-face image of lamina cribrosa where the complex structure of pores (dark) and beams (white) is clearly visible.

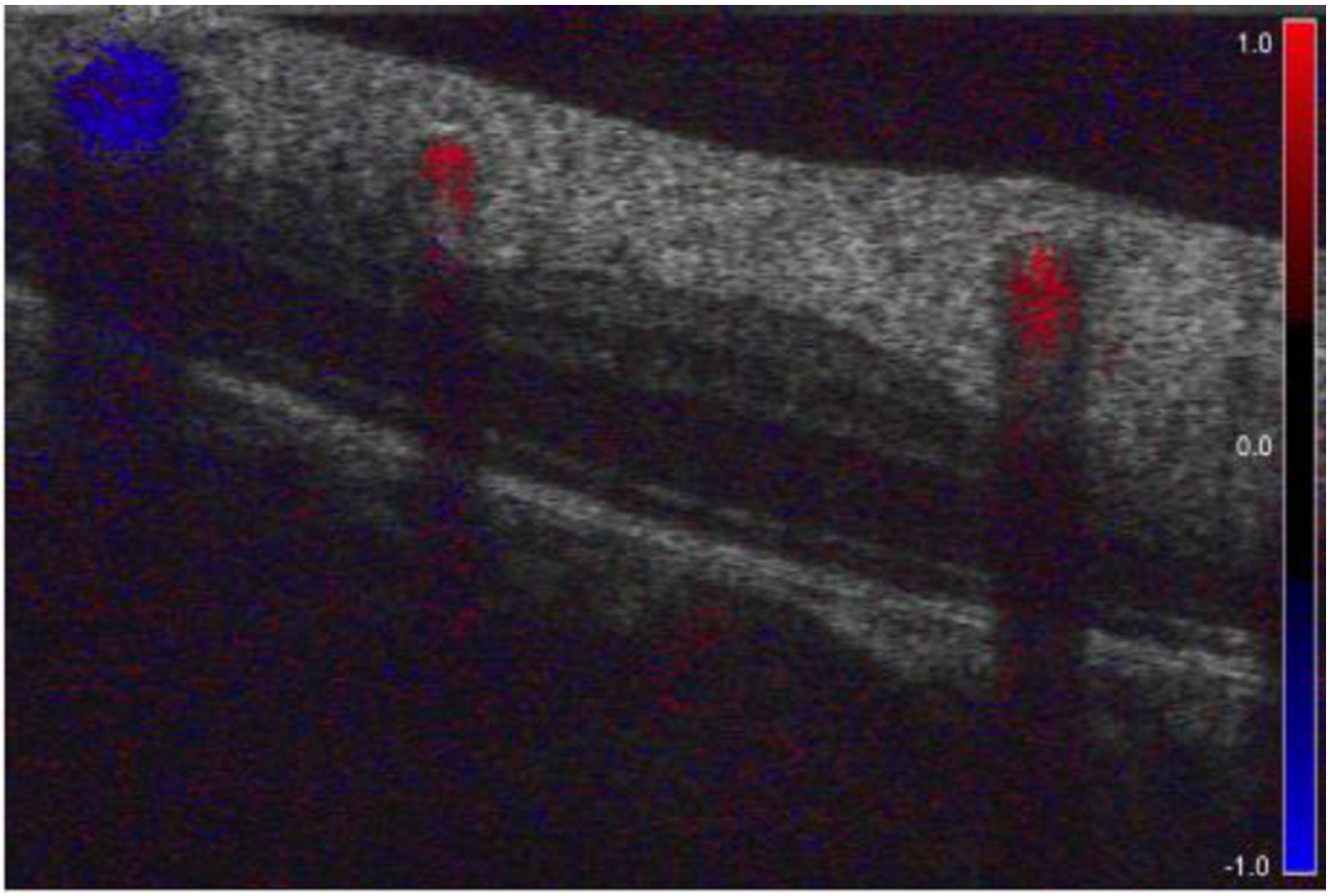

Figure 7.

Doppler OCT cross-section of the retina. The lumen of retinal vessels is filled with color that corresponds with the direction and velocity of blood flow. Blockage of the light beam results in vertically elongated shadows underneath the vessels.